Journal of Materials Chemistry A

COMMUNICATION

View Article Online
View Journal | View Issue

Cite this: J. Mater. Chem. A, 2015, 3, 17977

Received 7th June 2015
Accepted 3rd August 2015

DOI: 10.1039/c5ta04105h

www.rsc.org/MaterialsA

Enhanced photoelectrochemical water oxidation on a $BiVO_4$ photoanode modified with multi-functional layered double hydroxide nanowalls†

Wanhong He,[a] Ruirui Wang,[a] Lu Zhang,[a] Jie Zhu,[b] Xu Xiang*[a] and Feng Li[a]

A $BiVO_4$ photoanode was modified with a multi-functional layered double hydroxide (LDH) nanowall overlayer for PEC water oxidation. The composite photoanode exhibits a tremendous cathodic shift of the onset potential (~540 mV) and more than 2-fold enhancement in the oxidation efficiency and IPCE value.

The efficient harvest of solar energy and subsequent conversion into forms that can be used through green and sustainable ways are highly desired.[1] Photoelectrochemical (PEC) splitting of water or carbon dioxide reduction on the photoelectrodes can directly convert solar energy into clean fuels in the form of H_2 or hydrocarbon compounds, which received considerable attention in the last decades.[2] To achieve the overall water splitting, the water oxidation half-reaction is a bottleneck which needs to be overcome since it is a four-proton-coupled multi-electron process.[3,4] Consequently, the design of highly efficient photoanodes is the key to improve the PEC water splitting performance. However, the performance of photoanodes is limited by several critical factors such as the sluggish kinetics for water oxidation, the slow transport of carriers, and the insufficient utilization of solar light.[5] Combining semiconductor photoanodes with the functional materials which act as a water oxidation catalyst (WOC) or have a narrow band gap has been illustrated to be an effective way for improving the PEC performance of photoanodes. For instance, the deposition with Co–Pi or Co, Ni-oxides on the surface of the $BiVO_4$, Fe_2O_3 and Ta_3N_5 photoanodes can improve the PEC performance.[6–10] The combination of narrow-band-gap semiconductor WO_3 and $BiVO_4$ can increase the photocurrent significantly by facilitating the transfer of photo-generated carriers.[11]

Layered double hydroxides (LDHs) are a class of anionic clays in which various cations can be stabilized in the octahedral sites within the layers of LDHs.[12] LDHs can be used themselves as heterogeneous catalysts upon incorporating active components into their lattices.[13] Recently, LDHs containing Co, Fe, Mn and Ni have been reported to be high efficiency electrochemical water oxidation catalysts (WOCs).[14–18] It was observed that the LDH film by *in situ* growth onto a metal substrate presented higher oxygen-evolving reaction (OER) activity than that in the form of powder, owing to the highly oriented nanowall structure.[19] Except acting as WOCs, several kinds of LDHs played a role of photocatalysts for dye degradation or water splitting.[20–22] It is assumed that LDHs could be considered as "doped semiconductors" to promote the absorption and utilization of visible light.[21]

The rational assembly of photo-sensitizers and WOCs simultaneously onto the semiconductor photoanodes is still a challenging mission although great effort has been made.[23,24] Consequently, the effective integration of multi-functionality upon modifying a photoanode is of great desire.[25] Inspired by the catalytic and light-absorption characteristics of LDH itself, we modified the $BiVO_4$ photoanode with CoAl-LDH which could possess multiple functionalities and a unique two-dimensional (2D) structure as well. The LDH@$BiVO_4$ photoanode exhibited significant enhancement in PEC performance compared to the pristine $BiVO_4$. The IPCE value at 400 nm of the composite photoanode is twice higher than that of the pure one owing to the composite structure.

The XRD patterns of the photoanodes are shown in Fig. 1A. The reflections (at $2\theta = 18.8$ and 28.9 degrees) in the pattern of $BiVO_4$ can be assigned to monoclinic scheelite $BiVO_4$ (JCPDS no. 75-1866) besides those from the FTO substrate. The monoclinic phase of $BiVO_4$ was further determined by the bandgap analyzed below. No other crystalline phase like V_2O_5 or Bi_2O_3 was detected. After the growth of CoAl-LDH, several new reflections appear, which are consistent with the characteristic ones (003), (006), and (009) of LDH.[26] The relatively low intensity of reflection (003) indicates that the LDH could grow in a certain

[a]State Key Laboratory of Chemical Resource Engineering, Beijing University of Chemical Technology, Beijing 100029, PR China. E-mail: xiangxu@mail.buct.edu.cn
[b]Jiangsu Key Laboratory of Advanced Catalytic Materials and Technology, Changzhou University, 213164, PR China

† Electronic supplementary information (ESI) available: Experimental details, XRD patterns, optical bandgap of $BiVO_4$, XPS spectra, SEM images, and additional current–voltage curves. See DOI: 10.1039/c5ta04105h

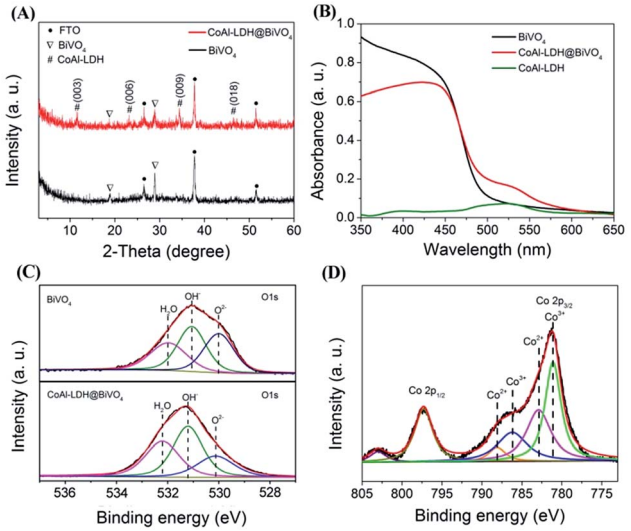

Fig. 1 (A) XRD patterns of the photoanodes; (B) UV-vis absorption spectra of the photoanodes; (C) XPS O1s spectra of $BiVO_4$ and LDH@$BiVO_4$ photoanodes; (D) XPS Co2p spectra of the LDH@$BiVO_4$ photoanode.

oriented way on the substrate.[19,27] As a control, the $Co(OH)_2$ was grown onto the $BiVO_4$. The XRD pattern does not present the reflections of cobalt hydroxide phases since their reflections are overlapped with those of $BiVO_4$ (Fig. S1†).

The UV-vis absorption behaviors of the photoanodes were investigated (Fig. 1B). The absorption edge of $BiVO_4$ is at ~490 nm. The bandgap of the $BiVO_4$ was estimated to be ~2.5 eV (Fig. S2†), which is close to the value of the monoclinic phase reported.[28] The XRD characterization and bandgap estimation verify that the monoclinic phase of $BiVO_4$ was synthesized. As to the LDH@$BiVO_4$ composite photoanode, the absorbance is increased in the visible range of 480–570 nm after the modification of LDH on $BiVO_4$. It was reported that the bandgap of $BiVO_4$ and CoAl-LDH is around 2.4 eV and 2.2 eV, respectively.[26,29] This is consistent with the UV-vis absorption results that LDH has stronger absorbance in the longer wavelength region. To further prove the contribution of absorption in the wavelength of 480–570 nm, the CoAl-LDH@FTO sample was measured. One can observe the obvious absorption in the region of 480–570 nm, which is in accordance with the enhanced absorption of LDH@$BiVO_4$ in the same region. It is a clear indication that the stronger absorption in this region comes from CoAl-LDH itself. This character may render LDH@$BiVO_4$ better utilization to the visible light with a longer wavelength.

To confirm the surface properties and chemical valence of the photoanodes, XPS measurements were achieved. The O1s core level was shown in Fig. 1C. Both the $BiVO_4$ and CoAl-LDH@$BiVO_4$ photoanodes can be fitted into three peaks. The peaks can be assigned to O^{2-}, OH^- species and adsorbed water, respectively, from the lower to the higher binding energy (B.E.).[30] The area ratio of OH^-/O^{2-} species is higher in CoAl-LDH@$BiVO_4$ than that in $BiVO_4$. It is attributable to the double hydroxides growth on the surface of $BiVO_4$. The valences of Co species in the CoAl-LDH@$BiVO_4$ were analyzed from the Co2p core level spectra (Fig. 1D). The spectra in the $Co2p_{3/2}$ region can be deconvoluted into four peaks. The peaks at 781.1 eV and 782.9 eV are ascribed to Co^{3+} and Co^{2+} species, respectively.[19] The peaks at the higher B.E. value of 786.1 eV and 788.1 eV are due to the Co^{3+} and Co^{2+} satellite, respectively. It is an indication that the Co^{2+} and Co^{3+} species co-exist in the as-grown CoAl-LDH. In contrast, the O1s XPS spectra of $Co(OH)_2$@$BiVO_4$ were measured (Fig. S3A†). Similar to the LDH, the peak associated with the OH^- has the highest intensity. In addition, the ratio of Co^{2+} to Co^{3+} species was calculated according to the integral peak areas of XPS spectra (Fig. S3B†). The ratio of Co^{2+} to Co^{3+} is 1.38, suggesting that the Co^{2+} species is dominant in the cobalt hydroxide overlayer. XPS spectra of Bi4f and V2p were also studied (Fig. S4†). The $BiVO_4$ photoanode presents the Bi and V signals from the respective core level spectra, whose B.E. values agree with the reported ones.[31] After the growth of LDH on $BiVO_4$, no signals were detected in the Bi4f and V2p spectra. This suggests that the surface of $BiVO_4$ is covered by LDH completed and the LDH layer is thick enough.

It is reported that the PEC performance of photoanodes is closely related to their structure at a micro/mesoscopic scale.[32] The morphology and microstructure of $BiVO_4$ and composite photoanodes were characterized by SEM and TEM. The $BiVO_4$ presents a particulate morphology with an irregular and rough appearance (Fig. 2A and C). The particles have sizes of 300–400 nm and grow on the FTO substrate non-continuously. The surface of the $BiVO_4$ photoanode is entirely covered by the quasi-vertically oriented nanosheets after CoAl-LDH is grown

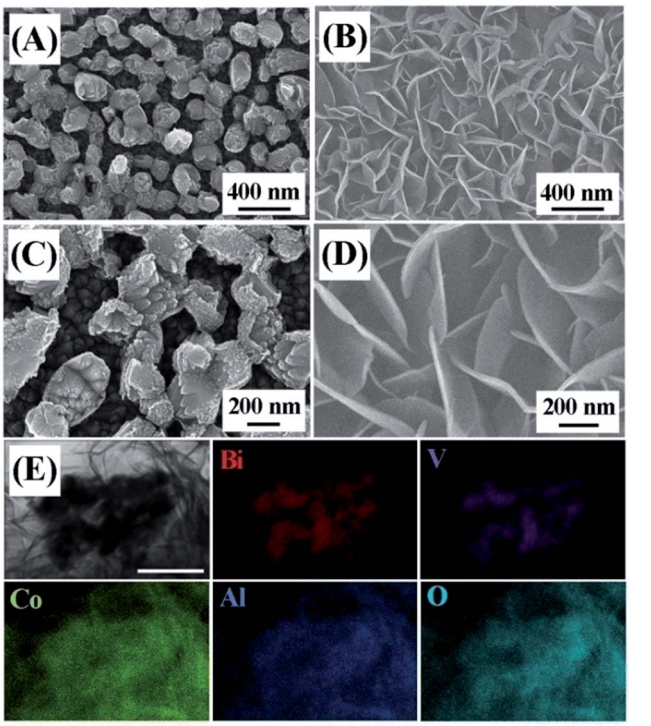

Fig. 2 SEM images of the photoanodes, (A) and (C) $BiVO_4$, (B) and (D) LDH@$BiVO_4$, (E) TEM image and EDS mappings of LDH@$BiVO_4$. The scale in (E) is 500 nm.

(Fig. 2B and D). The nanosheets interconnect in different orientations to form the interpenetrated nanowalls, similar to a previous report on ZnCo-LDH grown on a conductive substrate.[18] The nanosheets have a thickness of ~20 nm, far thinner than the lateral sizes. The thin 2D structure is beneficial to the transport of carriers during PEC reactions. The side-view from the cross-section of CoAl-LDH grown on the FTO clearly shows that the nanosheets stack from different angles and form a network-like structure (Fig. S5†).

It is worth noting that the thickness of the LDH nanowall (~4 μm) is thicker than that of the known catalyst layer commonly decorated onto the surface of photoanodes.[33] The thick layer may increase the light absorption since CoAl-LDH has the characteristic of visible-light-absorbing. As to the control $Co(OH)_2$@$BiVO_4$, the SEM images show the nanorod morphology with the widths of 70–130 nm and lengths of 400–1000 nm (Fig. S6†). Different from the growth mode of LDH nanosheets, the nanorods are lying down on the $BiVO_4$. This orientation could not facilitate the efficient transport of photogenerated carriers.

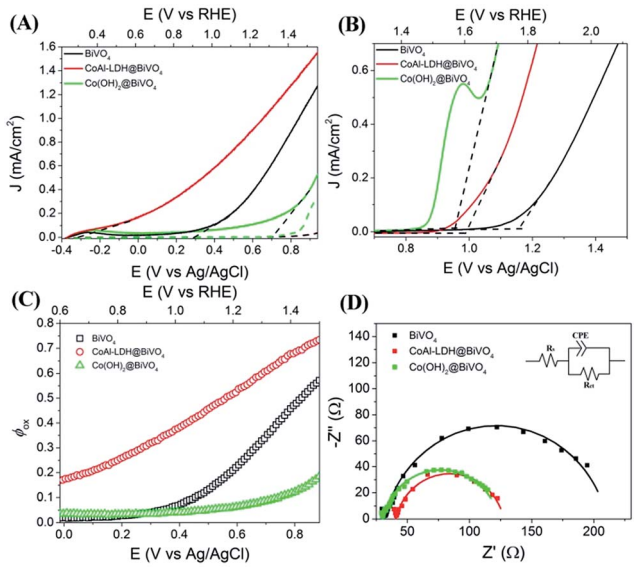

Fig. 3 (A) Current–voltage curves of the photoanodes under illumination (solid line) and in the dark (dashed line); (B) dark current–voltage curves in the higher potential range; (C) the oxidation efficiency of the surface-reaching holes injected into the solution species (ϕ_{ox}); (D) Nyquist plots of the photoanodes under illumination. Inset: the corresponding equivalent circuit. R_{ct} is the charge transfer resistance across the electrode/electrolyte interface, R_s is the solution resistance, and CPE is the constant phase component.

The microstructure and elemental distribution of CoAl-LDH@$BiVO_4$ are further revealed by the TEM (Fig. 2E) and EDS mappings. The elemental mappings on Bi, V, Co, Al and O display that the $BiVO_4$ particles are thoroughly encapsulated by network-like LDH nanosheets. The Bi and V elements distribute in the core region and the Co and Al elements in the surrounding. The EDS mapping analyses are consistent with the SEM observation, where no $BiVO_4$ particles are observed in the LDH@$BiVO_4$ composite photoanode.

The PEC measurements were achieved to disclose the functional roles of LDH when coupled with $BiVO_4$. The current–voltage behaviors of the photoanodes under illumination were studied. The onset potential was defined as the potential at the intersection point of the tangent at a maximum slope of photocurrent and the dark current curve (Fig. S7†).[34,35] The photocurrent onset potential of $BiVO_4$ here is similar to those reported previously.[36,37] Compared to the pristine $BiVO_4$, the onset potential of CoAl-LDH@$BiVO_4$ significantly reduces from 0.90 V to 0.36 V with a cathodic shift of 540 mV (Fig. 3A and Table 1). This cathodic shift value is the highest amongst all reported ones, in which $BiVO_4$ photoanodes were decorated with cobalt-, nickel-, or iron-containing WOC.[8,38] Furthermore, the onset potential of CoAl-LDH@$BiVO_4$ is lower than that of the Co–Pi decorated $BiVO_4$ photoanode.[7] In the control experiment, the current–voltage curve of $Co(OH)_2$@$BiVO_4$ was measured. The onset potential shows an anodic shift of ~400 mV and the photocurrent dramatically deceases. It clearly indicates that $Co(OH)_2$ has a severe negative effect on the PEC performance. The dark current–voltage curves reveal the electrochemical water oxidation properties, which could reflect the catalytic role of the LDH layer (Fig. 3B and Table 1). The CoAl-LDH@$BiVO_4$ and $Co(OH)_2$@$BiVO_4$ photoanodes present cathodic shifts of 170 and 200 mV, respectively. This finding confirms that both CoAl-LDH and $Co(OH)_2$ act as WOC to decrease the onset potential. Furthermore, the $Co(OH)_2$@$BiVO_4$ has a lower oxygen-evolving onset potential than CoAl-LDH@$BiVO_4$. However, the PEC performance of the latter greatly outperforms the former, indicating that the electrochemical catalytic ability of WOC is not a dominating factor for PEC performance.[39] Furthermore, the CoAl-LDH grown directly on the FTO hardly shows obvious photocurrent (Fig. S8†). This finding indicates that CoAl-LDH itself contributes little to the photocurrent of water oxidation.

The efficiency of substrate oxidation by surface-reaching holes (ϕ_{ox}) is related to photogenerated electron–hole recombination on the surface.[6,8] The ϕ_{ox} values of the photoanodes are calculated and shown in Fig. 3C (the details for ϕ_{ox} calculation

Table 1 The shift of the onset potential for water oxidation and charge transfer resistance of the photoanodes

Samples	E_{onset} under illumination (V *vs.* RHE)	E_{onset} shift under illumination (mV)	E_{onset} shift in the dark (mV)	R_{ct} (Ω)
$BiVO_4$	0.90	—	—	175
CoAl-LDH@$BiVO_4$	0.36	540 (cathodic)	170 (cathodic)	87
$Co(OH)_2$@$BiVO_4$	1.30	400 (anodic)	200 (cathodic)	93

are given in the ESI, the Experimental section and Fig. S9†). The CoAl-LDH@$BiVO_4$ presents higher ϕ_{ox} during the potential range from 0.6–1.5 V compared with $BiVO_4$. For example, the former has a ϕ_{ox} of 54.5% at 1.23 V, twice higher than that of the latter (24.6%). The much higher ϕ_{ox} indicates that more holes can be transported to the surface and efficiently oxidize water under illumination. In contrast, $Co(OH)_2$@$BiVO_4$ has a much inferior ϕ_{ox} compared with $BiVO_4$. To explore the charge transport properties, the electrochemical impedance spectra (EIS) were measured.[40] From the Nyquist plots (Fig. 3D), the charge transfer resistances (R_{ct}) across the electrode/electrolyte interface were calculated and compared. The R_{ct} of CoAl-LDH@$BiVO_4$ is smaller than that of $BiVO_4$ (Table 1), suggestive of the superior charge transport capability of the former. It is noticed that the R_{ct} values of CoAl-LDH@$BiVO_4$ and $Co(OH)_2$@$BiVO_4$ have a slight difference. However, the CoAl-LDH@$BiVO_4$ has a much better PEC performance than the control. It indicates that the performance is affected by other factors besides the charge transport properties.

The incident photon-to-current efficiency (IPCE) value is a critical index to study light conversion efficiency. The CoAl-LDH@$BiVO_4$ presents a higher IPCE value than $BiVO_4$ from UV extending to the visible region. The IPCE of the former reaches 37% at 400 nm, which is 2.2 times as high as the latter (Fig. 4A). The IPCE value of $BiVO_4$ drops down to zero at 520 nm, whereas the IPCE of CoAl-LDH@$BiVO_4$ does not decrease to zero until around 600 nm (inset of Fig. 4A). The photon-to-current conversion efficiency is enhanced, which could be caused by the composite structure and the light-absorbing properties of LDH. The absorbed photon-to-current efficiency (APCE) of CoAl-LDH@$BiVO_4$ at 400 nm is 47%, which is 2.4 times as high as that of $BiVO_4$ (Fig. 4B) and also higher than that of the CoPi-decorated $BiVO_4$ photoanode reported.[6] The APCE results indicate that the composite photoanode may utilize the absorbed light more efficiently.[41]

As to the composite photoanodes consisting of two functional materials, it has been reported that the PEC performance is largely related to the separation of photogenerated electron–hole across the interface.[7,26,42] The fluorescent process is one of the recombination ways for the photogenerated carriers and thus has a negative effect on the carrier separation. We studied the photoluminescence (PL) properties of the photoanodes (Fig. 5). The CoAl-LDH grown on the FTO substrate exhibits an intensive fluorescence emission band of 420–480 nm whereas

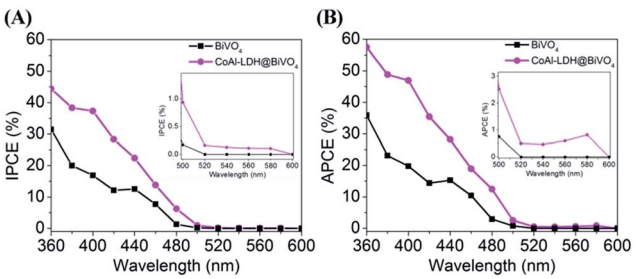

Fig. 4 IPCE (A) and APCE (B) of $BiVO_4$ and LDH@$BiVO_4$ photoanodes measured by monochromatic light.

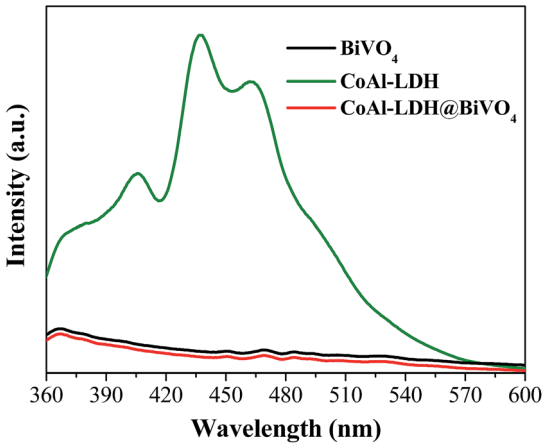

Fig. 5 Fluorescence spectra of $BiVO_4$, LDH grown on FTO and LDH@$BiVO_4$.

the $BiVO_4$ shows little fluorescence signals. The CoAl-LDH@$BiVO_4$ photoanode has almost complete fluorescence quenching. This finding verifies that the fluorescence-associated recombination in CoAl-LDH@$BiVO_4$ is greatly suppressed, which could favor the electron–hole separation.

According to the results stated above, a tentative mechanism for PEC water oxidation on the CoAl-LDH@$BiVO_4$ photoanode was proposed (Fig. 6). Firstly, the energy level matching between CoAl-LDH and $BiVO_4$ facilitates the transport of photo-generated electrons to the FTO and holes to the surface.[11,42] Secondly, the dual light-absorbing properties of the composite photoanode improve the utilization of light irradiated. That is to say, the wider-bandgap $BiVO_4$ (2.4 eV) absorbs shorter visible light and the narrower-bandgap CoAl-LDH (2.2 eV) absorbs longer visible light, evidenced by UV-vis absorption and IPCE measurements. This configuration of two materials with different bandgaps favors better utilization of solar light.[43] Also, the thick layer of LDH may absorb more light. Besides, the highly dispersed Co^{2+}/Co^{3+} species within the LDH nanosheets can be oxidized to higher valence Co^{3+}/Co^{4+}, which catalyze water oxidation and expedite the kinetics.[44,45] Last but not least,

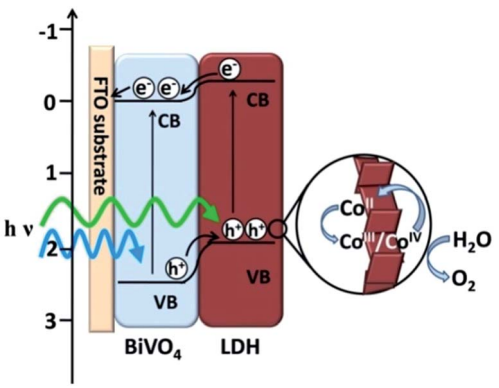

Fig. 6 Schematic mechanism of LDH@$BiVO_4$ for PEC water oxidation (VB: valence band, CB: conduction band, the unit of the scale is in volt *vs.* NHE).

the unique nanowall consisting of LDH 2D nanosheets could shorten the hole diffusion distance and facilitate the transport of holes to the surface. Meanwhile, the nanowall structure makes the catalytic sites on the LDH to be exposed more efficiently compared to the stacked or lying structure. Consequently, the significant enhancement in PEC performance of the CoAl-LDH@$BiVO_4$ photoanode can be ascribed to the catalysis/light-absorbing/2D structure triple functionality.

Conclusions

A $BiVO_4$ photoanode was successfully modified with an overlayer of CoAl-LDH. The 2D LDH nanosheets with a thickness of ~20 nm interconnected to form a network-like nanowall. Such a composite photoanode exhibits a significant cathodic shift of the onset potential (~540 mV), which is the largest shift amongst all WOC@$BiVO_4$ photoanodes ever reported. This finding is attributed to the electrocatalytic role of CoAl-LDH. The photocurrent is enhanced and the oxidation efficiency (at 1.23 V) of holes is two times higher than that of pristine $BiVO_4$. Furthermore, 2-fold enhancement in the IPCE value (at 400 nm) is achieved. The LDH also presents more light absorption in the longer wavelength region of 480–570 nm. Besides, the 2D nanosheet structure enhances the carrier-transporting properties, promoting the diffusion of holes to the surface. This work opens up a new pathway to improve the PEC performance of photoanodes by functionality-integrated structural design. The LDH@semiconductor structure could be further optimized by interfacial engineering for constructing high efficiency photoanodes.

Acknowledgements

This work was supported by the 973 Program (Grant no. 2011CBA00506), the National Natural Science Foundation of China, Beijing Natural Science Foundation (Grant no. 2152022), the Program for Changjiang Scholars and Innovative Research Team in University (Grant no. IRT1205), the Fundamental Research Funds for the Central Universities (YS1406) and Jiangsu Key Laboratory of Advanced Catalytic Materials and Technology (Grant no. BM2012110).

Notes and references

1 N. S. Lewis and D. G. Nocera, *PNAS*, 2006, **103**, 15729–15735.
2 M. Gratzel, *Nature*, 2001, **414**, 338–344.
3 D. G. Nocera, *Acc. Chem. Res.*, 2012, **45**, 767–776.
4 F. Song, Y. Ding, B. Ma, C. Wang, Q. Wang, X. Du, S. Fu and J. Song, *Energy Environ. Sci.*, 2013, **6**, 1170–1184.
5 H. M. Chen, C. K. Chen, R.-S. Liu, L. Zhang, J. Zhang and D. P. Wilkinson, *Chem. Soc. Rev.*, 2012, **41**, 5654–5671.
6 M. Zhou, J. Bao, W. Bi, Y. Zeng, R. Zhu, M. Tao and Y. Xie, *ChemSusChem*, 2012, **5**, 1420–1425.
7 M. Zhong, T. Hisatomi, Y. Kuang, J. Zhao, M. Liu, A. Iwase, Q. Jia, H. Nishiyama, T. Minegishi, M. Nakabayashi, N. Shibata, R. Niishiro, C. Katayama, H. Shibano, M. Katayama, A. Kudo, T. Yamada and K. Domen, *J. Am. Chem. Soc.*, 2015, **137**, 5053–5060.
8 D. K. Zhong, S. Choi and D. R. Gamelin, *J. Am. Chem. Soc.*, 2011, **133**, 18370–18377.
9 K. Sivula, F. Le Formal and M. Grätzel, *ChemSusChem*, 2011, **4**, 432–449.
10 G. Liu, J. Shi, F. Zhang, Z. Chen, J. Han, C. Ding, S. Chen, Z. Wang, H. Han and C. Li, *Angew. Chem., Int. Ed.*, 2014, **53**, 7295–7299.
11 P. M. Rao, L. Cai, C. Liu, I. S. Cho, C. H. Lee, J. M. Weisse, P. Yang and X. Zheng, *Nano Lett.*, 2014, **14**, 1099–1105.
12 Q. Wang and D. O'Hare, *Chem. Rev.*, 2012, **112**, 4124–4155.
13 X. Xiang, H. I. Hima, H. Wang and F. Li, *Chem. Mater.*, 2008, **20**, 1173–1182.
14 X. Zou, A. Goswami and T. Asefa, *J. Am. Chem. Soc.*, 2013, **135**, 17242–17245.
15 M. Gong, Y. Li, H. Wang, Y. Liang, J. Z. Wu, J. Zhou, J. Wang, T. Regier, F. Wei and H. Dai, *J. Am. Chem. Soc.*, 2013, **135**, 8452–8455.
16 Y. Zhang, B. Cui, C. Zhao, H. Lin and J. Li, *Phys. Chem. Chem. Phys.*, 2013, **15**, 7363–7369.
17 F. Song and X. Hu, *J. Am. Chem. Soc.*, 2014, **136**, 16481–16484.
18 M. Shao, F. Ning, M. Wei, D. G. Evans and X. Duan, *Adv. Funct. Mater.*, 2014, **24**, 580–586.
19 Y. Li, L. Zhang, X. Xiang, D. Yan and F. Li, *J. Mater. Chem. A*, 2014, **2**, 13250–13258.
20 S. J. Kim, Y. Lee, D. K. Lee, J. W. Lee and J. K. Kang, *J. Mater. Chem. A*, 2014, **2**, 4136–4139.
21 C. G. Silva, Y. Bouizi, V. Fornés and H. García, *J. Am. Chem. Soc.*, 2009, **131**, 13833–13839.
22 X. Xiang, F. Li and Z. Huang, *Reviews in Advanced Sciences and Engineering*, 2014, **3**, 158–171.
23 X. Xiang, J. Fielden, W. Rodriguez-Cordoba, Z. Huang, N. Zhang, Z. Luo, D. G. Musaev, T. Lian and C. L. Hill, *J. Phys. Chem. C*, 2013, **117**, 918–926.
24 Y. Gao, X. Ding, J. Liu, L. Wang, Z. Lu, L. Li and L. Sun, *J. Am. Chem. Soc.*, 2013, **135**, 4219–4222.
25 W. He, Y. Yang, L. Wang, J. Yang, X. Xiang, D. Yan and F. Li, *ChemSusChem*, 2015, **8**, 1568–1576.
26 Y. Dou, S. Zhang, T. Pan, S. Xu, A. Zhou, M. Pu, H. Yan, J. Han, M. Wei, D. G. Evans and X. Duan, *Adv. Funct. Mater.*, 2015, **25**, 2243–2249.
27 J. Zhao, M. Shao, D. Yan, S. Zhang, Z. Lu, Z. Li, X. Cao, B. Wang, M. Wei, D. G. Evans and X. Duan, *J. Mater. Chem. A*, 2013, **1**, 5840–5846.
28 S. J. A. Moniz, J. Zhu and J. Tang, *Adv. Energy Mater.*, 2014, **4**, 1301590.
29 J. A. Seabold and K.-S. Choi, *J. Am. Chem. Soc.*, 2012, **134**, 2186–2192.
30 K. M. H. Young and T. W. Hamann, *Chem. Commun.*, 2014, **50**, 8727–8730.
31 N. Myung, S. Ham, S. Choi, Y. Chae, W.-G. Kim, Y. J. Jeon, K.-J. Paeng, W. Chanmanee, N. R. de Tacconi and K. Rajeshwar, *J. Phy. Chem. C*, 2011, **115**, 7793–7800.
32 M. Zhou, X. W. Lou and Y. Xie, *Nano Today*, 2013, **8**, 598–618.

33 G. M. Carroll, D. K. Zhong and D. R. Gamelin, *Energy Environ. Sci.*, 2015, **8**, 577–584.
34 D. K. Zhong, M. Cornuz, K. Sivula, M. Gratzel and D. R. Gamelin, *Energy Environ. Sci.*, 2011, **4**, 1759–1764.
35 D. Cao, W. Luo, J. Feng, X. Zhao, Z. Li and Z. Zou, *Energy Environ. Sci.*, 2014, **7**, 752–759.
36 L. Chen, F. M. Toma, J. K. Cooper, A. Lyon, Y. Lin, I. D. Sharp and J. W. Ager, *ChemSusChem*, 2015, **8**, 1066–1071.
37 Y. Ma, S. R. Pendlebury, A. Reynal, F. Le Formal and J. R. Durrant, *Chem. Sci.*, 2014, **5**, 2964–2973.
38 T. W. Kim and K.-S. Choi, *Science*, 2014, **343**, 990–994.
39 Y.-C. Wang, C.-Y. Chang, T.-F. Yeh, Y.-L. Lee and H. Teng, *J. Mater. Chem. A*, 2014, **2**, 20570–20577.
40 B. Klahr, S. Gimenez, F. Fabregat-Santiago, J. Bisquert and T. W. Hamann, *Energy Environ. Sci.*, 2012, **5**, 7626–7636.
41 K. Fuku, N. Wang, Y. Miseki, T. Funaki and K. Sayama, *ChemSusChem*, 2015, **8**, 1593–1600.
42 S. Ho-Kimura, S. J. A. Moniz, A. D. Handoko and J. Tang, *J. Mater. Chem. A*, 2014, **2**, 3948–3953.
43 L. Han, F. F. Abdi, R. van de Krol, R. Liu, Z. Huang, H.-J. Lewerenz, B. Dam, M. Zeman and A. H. M. Smets, *ChemSusChem*, 2014, **7**, 2832–2838.
44 M. Barroso, A. J. Cowan, S. R. Pendlebury, M. Grätzel, D. R. Klug and J. R. Durrant, *J. Am. Chem. Soc.*, 2011, **133**, 14868–14871.
45 C. L. Farrow, D. K. Bediako, Y. Surendranath, D. G. Nocera and S. J. L. Billinge, *J. Am. Chem. Soc.*, 2013, **135**, 6403–6406.